ARTHRITIS & RHEUMATISM
Vol. 58, No. 1, January 2008, pp 240–250
DOI 10.1002/art.23143


# A Biomarker-Based Mathematical Model to Predict Bone-Forming Potency of Human Synovial and Periosteal Mesenchymal Stem Cells

Cosimo De Bari,[1] Francesco Dell'Accio,[1] Alexandra Karystinou,[1] Pascale V. Guillot,[2] Nicholas M. Fisk,[2] Elena A. Jones,[3] Dennis McGonagle,[3] Ilyas M. Khan,[4] Charles W. Archer,[4] Thimios A. Mitsiadis,[5] Ana Nora Donaldson,[1] Frank P. Luyten,[6] and Costantino Pitzalis[1]

***Objective.*** **To develop a biomarker-based model to predict osteogenic potency of human mesenchymal stem cells (MSCs) from synovial membrane and periosteum.**

***Methods.*** **MSC populations were derived from adult synovium and periosteum. Phenotype analysis was performed by fluorescence-activated cell sorting and real-time reverse transcriptase–polymerase chain reaction (RT-PCR). Telomere lengths were determined by Southern blot analysis. In vitro osteogenesis was assessed quantitatively by measurements of alkaline phosphatase activity and calcium deposits. To investigate bone formation in vivo, MSCs were seeded onto osteoinductive scaffolds and implanted subcutaneously in nude mice. Bone was assessed by histology, and the human origin investigated by in situ hybridization for human Alu genomic repeats. Quantitation was achieved by histomorphometry and real-time RT-PCR for human osteocalcin. Analysis at the single-cell level was performed with clonal populations obtained by limiting dilution. Multiple regressions were used to explore the incremental predictive value of the markers.**

***Results.*** **Periosteal MSCs had significantly greater osteogenic potency than did synovial MSCs inherent to the single cell. Bone was largely of human origin in vivo. Within the same tissue type, there was variability between different donors. To identify predictors of osteogenic potency, we measured the expression levels of osteoblast lineage genes in synovial and periosteal clonal MSCs prior to osteogenic treatment. We identified biomarkers that correlated with osteogenic outcome and developed a mathematical model based on type I collagen and osteoprotegerin expression that predicts the bone-forming potency of MSC preparations, independent of donor-related variables and tissue source.**

***Conclusion.*** **Our findings indicate that our quality-control mathematical model estimates the bone-forming potency of MSC preparations for bone repair.**

Increasing evidence supports the clinical use of stem cells for tissue repair. A major concern is the large structural and clinical variability in outcome. Such variability is at least partly due to donor-related factors and the inconsistency of stem cell preparations. This problem has been highlighted by the recent publication of contrasting results in clinical trials of cardiac cell therapy (1).

The known osteogenic capacity of mesenchymal stem cells (MSCs) (2–5) makes bone repair a natural application of MSC preparations. MSC-based approaches to bone repair would circumvent clinical complications associated with the use of autologous bone

Supported by MRC grant G108/620 and IWT grant 000259. Dr. De Bari is a Fellow of the Medical Research Council, UK. Dr. Dell'Accio is a Fellow of the Arthritis Research Campaign, UK. Dr. Guillot's work was supported by Action Medical Research, UK.

[1]Cosimo De Bari, MD, PhD (current address: University of Aberdeen, Aberdeen, UK), Francesco Dell'Accio, MD, PhD (current address: Queen Mary, University of London, London, UK), Alexandra Karystinou, MSc, Ana Nora Donaldson, MSc, PhD, CStat, Costantino Pitzalis, MD, PhD, FRCP (current address: Queen Mary, University of London, London, UK): King's College London, London, UK; [2]Pascale V. Guillot, PhD, Nicholas M. Fisk, MBBS, PhD, FRCOG: Imperial College London, London, UK; [3]Elena A. Jones, PhD, Dennis McGonagle, PhD, FRCPI: University of Leeds, Leeds, UK; [4]Ilyas M. Khan, PhD, Charles W. Archer, PhD: Cardiff University, Cardiff, UK; [5]Thimios A. Mitsiadis, DDS, PhD, HDR: University of Zurich, Zurich, Switzerland; [6]Frank P. Luyten, MD, PhD: Katholieke Universiteit Leuven, Leuven, Belgium.

Address correspondence and reprint requests to Cosimo De Bari, MD, PhD, Professor of Translational Medicine, Department of Medicine & Therapeutics, Institute of Medical Sciences, Foresterhill, Aberdeen AB25 2ZD, UK. E-mail: c.debari@abdn.ac.uk.

Submitted for publication January 3, 2007; accepted in revised form September 28, 2007.

grafts, such as donor site morbidity and the long-term discomfort that accompanies bone harvest. Transplantation of allogeneic bone is also used, but is subject to disease transmission and host rejection. Proof-of-concept studies in humans support the clinical utility of MSCs for bone repair (6–8). The incorporation of MSCs into osteoinductive scaffolds accelerates the formation of bone with biomechanical properties equivalent to bone grafts in vivo (9).

Donor-associated factors and MSC preparation protocols influence the bone-forming capacity of MSCs (10). In addition, MSCs isolated from different tissues have distinct differentiation properties (11–15). The resulting variability limits standardization of MSC-based approaches to bone repair and impedes comparison of clinical study outcomes. There is, therefore, a pressing clinical need for assays that allow quantitative estimation of the bone-forming potency of MSC preparations. Such potency assays would allow development of quality controls for efficacy of MSC preparations (16,17), a prerequisite for routine use in clinical practice.

In this study, we analyzed the variability in osteogenic potency of matched human MSC preparations from synovial membrane (SM) and periosteum and identified biomarkers that, using a mathematical formula modeled on the quantitative outcome of 2 independent assays of bone formation, predict the bone-forming potency of MSC preparations independently of donor-related variables and tissue source.

## MATERIALS AND METHODS

**Cell isolation and culture.** Samples of human periosteum (wet weight 10–50 mg) were harvested aseptically from the proximal medial tibia of 4 donors of various ages (24, 36, 58, and 83 years). Random biopsies of SM (wet weight 10–50 mg) were obtained aseptically from the knee joints of the same 4 donors. All specimens were obtained within 12 hours after death. Donors had no history of knee joint disorders and did not have active infections or tumors. Periosteal and synovial specimens from each donor were processed in parallel using the same protocol, as previously described (5). Cells were isolated and expanded in monolayer on plastic in growth medium (high-glucose Dulbecco's modified Eagle's medium [DMEM; Life Technologies, Gaithersburg, MD] containing 10% fetal bovine serum [selected lot from Life Technologies] and antibiotics [Life Technologies]) (5).

**Cell cloning.** Cell cloning was performed by limiting dilution as described elsewhere (4). First-passage synovial and periosteal cells were suspended in growth medium and plated at a density of 0.5 cells/well in 96-well, flat-bottomed culture plates. Cell populations arising from single cells were subcultured upon reaching confluence with serial 1:4 dilution passages.

**Telomere length assay.** Genomic DNA was extracted from passage 7 periosteal and synovial MSC monolayers using a standard protocol, and telomere lengths were determined semiquantitatively by Southern blotting using TeloTAGGG telomere length assay, according to the recommendations of the manufacturer (Roche, Indianapolis, IN). Mean telomere length was determined as described previously (18).

**Phenotyping of culture-expanded MSCs using 3-color flow cytometry.** Culture-expanded (passage 4 to passage 6) MSCs were used for flow cytometry at $10^5$ cells/test. Test antibodies were as follows: phycoerythrin (PE)–conjugated low-affinity nerve growth factor receptor (LNGFR)/p75, CD106 (vascular cell adhesion molecule 1), CD146 (Muc18), CD166 (activated leukocyte cell adhesion molecule), CD73/SH3 (all from PharMingen, San Diego, CA), CD105/SH2 (Serotec, Oxford, UK), fluorescein isothiocyanate (FITC)–conjugated CD45 (Dako, Carpinteria, CA), and CD13 (Serotec). D7-FIB–PE was labeled in-house from purified D7-FIB (Serotec). Hybridoma cells B4-78 against bone and liver isoforms of alkaline phosphatase were obtained from the Developmental Studies Hybridoma Bank (Iowa City, IA). Hybridoma supernatant was produced in-house, and antibody labeling was detected using secondary goat anti-mouse FITC (Serotec). Isotype-specific negative control antibodies were purchased from Serotec. Dead cells were gated out based on propidium iodide exclusion (Sigma, St. Louis, MO). All flow cytometry data were analyzed with WinMDI, version 8 software (Scripps Research Institute, La Jolla, CA).

**In vitro osteogenesis.** The in vitro osteogenesis assay was performed as described previously (5). Alkaline phosphatase activity was determined colorimetrically as described previously (4), using a commercially available kit (Thermo Electron Corporation, Waltham, MA). Protein content was determined by the Bradford method (Bio-Rad, Richmond, CA), using bovine serum albumin (Sigma) as standard. Alkaline phosphatase activity was expressed as arbitrary units per microgram of protein content. To determine calcium content, cell layers were rinsed twice with phosphate buffered saline and scraped off the dish in 0.5*N* HCl. The cell layers were extracted by shaking for 4 hours at 4°C, were centrifuged at 1,000*g* for 5 minutes, and the supernatant was used for calcium determination using a commercially available kit, according to the recommendations of the manufacturer (Thermo Electron Corporation). Total calcium was calculated from standard solutions and expressed as micrograms per microgram of protein content (determined in parallel wells).

**In vivo osteogenesis.** Animal experiments were performed in compliance with the UK Home Office and the Ethics Committee for Animal Research at the Katholieke Universiteit. MSCs were seeded onto the osteoinductive Collagraft matrix (NeuColl, Campbell, CA) and implanted subcutaneously into nude mice as described previously (4). Briefly, 3-$mm^3$ Collagraft cubes were wetted in DMEM, blotted onto a gauze compress, and immersed into 50 $\mu$l of MSC suspension ($10^5$ cells/$\mu$l in growth medium) to allow attachment of the cells to the Collagraft matrix. After 1 hour of incubation at 37°C, cells that did not attach to the Collagraft matrix but remained in suspension in the medium were counted and subtracted from the total number of seeded cells (5 million) to calculate the seeding efficiency as the percentage of cells that remained in the Collagraft matrix after 1 hour of incubation.

**Table 1.** Primers used for real-time RT-PCR analysis and sizes of PCR products*

| Gene | Primer sequence | Amplicon (bp) |
|---|---|---|
| $\beta$-actin | Forward 5′-CACGGCTGCTTCCAGCTC-3′<br>Reverse 5′-CACAGGACTCCATGCCCAG-3′ | 134 |
| GAPDH | Forward 5′-AACAGCGACACCCACTCCTC-3′<br>Reverse 5′-CATACCAGGAAATGAGCTTGACAA-3′ | 85 |
| Runx2 | Forward 5′-GCAGCACGCTATTAAATCCAAATT-3′<br>Reverse 5′-GGCACGAAGGCTCATCATTC-3′ | 115 |
| Osterix | Forward 5′-CCCCACCTCTTGCAACCA-3′<br>Reverse 5′-GGCTCCACCACTCCCTTCTAG-3′ | 102 |
| ALP | Forward 5′-CCCTTGACCCCCACAATGT-3′<br>Reverse 5′-GTTGTTCCTGTTGACCTCGTACTG-3′ | 80 |
| Type I collagen | Forward 5′-CAGCCGCTTCACCTACAGC-3′<br>Reverse 5′-TTTTGTATTCAATCACTGTCTTGCC-3′ | 85 |
| OPG | Forward 5′-GTGGACCACCCAGGAAACG-3′<br>Reverse 5′-CGGTCTTCCACTTTGCTGTACAG-3′ | 132 |
| Osteonectin | Forward 5′-TCTTCCCTGTACACTGGCAGTTC-3′<br>Reverse 5′-AACTGCTCCATGGGGATGGA-3′ | 115 |
| Osteopontin | Forward 5′-GCCGACCAAGGAAAACTCACTA-3′<br>Reverse 5′-CAGAACTTCCAGAATCAGCCTGTT-3′ | 107 |
| Osteocalcin | Forward 5′-CCTCACACTCCTCGCCCTATT-3′<br>Reverse 5′-CCCTCCTGCTTGGACACAAA-3′ | 117 |
| BSP | Forward 5′-AAACGAAGAAAGCGAAGCAGAA-3′<br>Reverse 5′-GCTGCCGTTGCCGTTTT-3′ | 94 |

* RT-PCR = reverse transcriptase–polymerase chain reaction; ALP = alkaline phosphatase; OPG = osteoprotegerin; BSP = bone sialoprotein.

The seeding efficiency was independent of cell type and routinely varied between 40% and 70%. The cell–Collagraft constructs were implanted subcutaneously into nude mice. At different time points postimplantation, mice were killed, and the constructs dissected. The explants were then cut in two, and one half was used for total RNA extraction and the other fixed overnight in 4% formaldehyde. Fixed samples were decalcified overnight in Decal (Serva, Heidelberg, Germany), paraffin-embedded, and sectioned (into 7-$\mu$m–thick sections) at 3 different levels.

**Histology and bone histomorphometry.** Sections were stained with hematoxylin and eosin (H&E) and then assessed qualitatively for the presence of bone tissue and quantitatively by bone histomorphometry. For each section, the total area and the area covered with bone tissue were measured using Scion Image (Scion, Frederick, MD). The amount of bone tissue was then calculated as a percentage of the total implant area.

**In situ hybridization for human-specific Alu genomic repeats.** In situ hybridization for human Alu genomic repeats was performed as described previously (19,20).

**Total RNA extraction and reverse transcriptase–polymerase chain reaction (RT-PCR) analysis.** Explants were homogenized in TRIzol reagent (Life Technologies) using a Polytron homogenizer. Total RNA was isolated using TRIzol, according to the recommendations of the manufacturer. After DNase treatment, complementary DNA (cDNA) samples were obtained by reverse transcription of 2 $\mu$g of total RNA (ThermoScript; Life Technologies) using oligo$(dT)_{20}$ as primer. Real-time quantitative PCR was carried out with SYBR Green using the Opticon real-time PCR cycler (MJ Research, San Francisco, CA). Gene expression of human cells within mouse tissue was evaluated using primers specific for human cDNA samples as described previously (4,21,22). Mouse bone was used to ensure specificity of the primers for human cDNA samples. Primer sequences are listed in Table 1.

**Statistical analysis.** Each assessment was performed on 2 or 3 cultures or constructs per cell source. Parametric data were analyzed using Student's *t*-test and are presented as the mean ± SD. Analysis of variance with Bonferroni adjustment for multiple comparisons was used to evaluate alkaline phosphatase activity over time in SM MSCs versus periosteal MSCs. Multiple regressions were used to explore the incremental predictive value of the markers, taking into account any significant interactions. Polynomial and logarithmic transformations of the markers were explored. Agreement of the measurements of calcium with the model was assessed using mixed linear regressions, to account for the effect of the donor, as well as the Bland and Altman method and intraclass

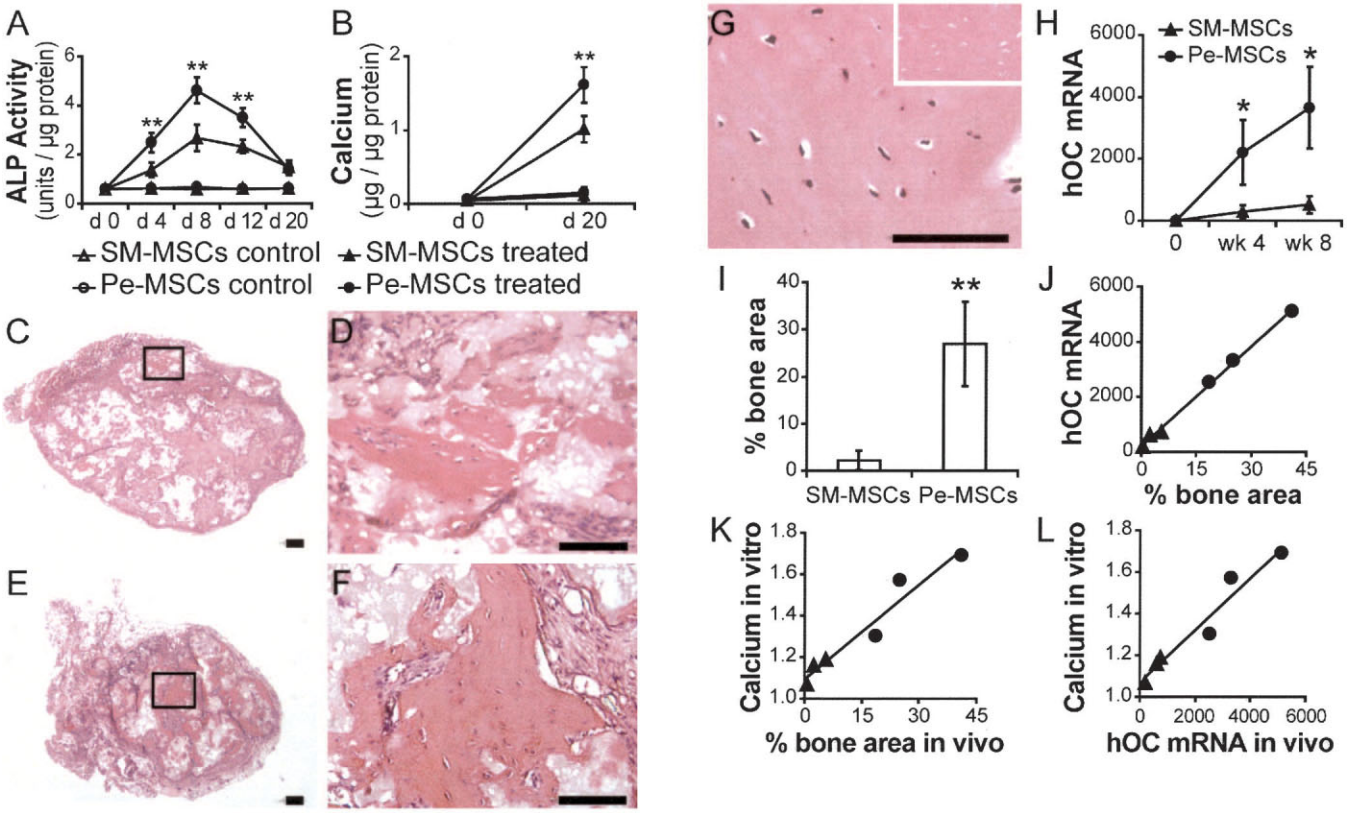


**Figure 1.** Osteogenic potency of synovial membrane (SM) mesenchymal stem cells (MSCs) and periosteal (Pe) MSCs. **A** and **B,** Osteogenesis in vitro. Human SM MSCs and periosteal MSCs were treated with osteogenic medium. Alkaline phosphatase (ALP) activity (**A**) was determined on days 0, 4, 8, 12, and 20, and MSC calcium deposition (**B**) was determined (in parallel wells) on days 0 and 20. Values are the mean ± SD of 4 donors. **C–L,** Bone formation in vivo. MSCs from 3 donors (ages 24, 36, and 83 years) were seeded onto Collagraft scaffolds, and the constructs implanted subcutaneously into nude mice. **C**, Hematoxylin and eosin (H&E) staining of SM MSCs 8 weeks after implantation. **D,** Higher-magnification view of the boxed area in **C**. **E,** H&E staining of periosteal MSCs 8 weeks after implantation. **F,** Higher-magnification view of the boxed area in **E**. **G,** Representative photomicrograph of an in situ hybridization for human Alu genomic repeats of a periosteal MSC construct at 8 weeks, counterstained with eosin. **Inset**, In situ hybridization for human Alu genomic repeats of mouse bone tissue used as a control, counterstained with eosin. Human nuclei are stained black. No nuclear counterstaining was performed, and therefore, Alu-negative nuclei are not visible. Bars = 100 $\mu$m. **H,** Quantification of the results of real-time quantitative reverse transcriptase–polymerase chain reaction for human osteocalcin (hOC) normalized to human $\beta$-actin. Expression of human OC was monitored in MSC monolayers and at 4 and 8 weeks after implantation of the constructs. The primers used were specific for human cDNA. The bone marker OC was barely detectable in the monolayer cultures, but OC levels increased progressively after 4 and 8 weeks in vivo. At both time points examined, the levels of human OC in periosteal MSC constructs were significantly higher than the levels in SM MSC constructs. Values are the mean ± SD of 3 donors. **I,** Quantification of in vivo bone formation assessed by histomorphometry. Values are the mean ± SD of 3 donors. **J,** Correlation between percent bone area and expression of human OC (normalized to human $\beta$-actin) at 8 weeks in vivo. **K,** Correlation between micrograms of calcium per microgram of protein content at 20 days in vitro and percent bone area at 8 weeks in vivo. **L,** Correlation between micrograms of calcium per microgram of protein content at 20 days in vitro and expression of human OC (normalized to human $\beta$-actin) at 8 weeks in vivo. Values in **J–L** are the mean. $* = P < 0.05$; $** = P < 0.01$, versus SM MSCs.

correlation coefficients (ICCs), and 95% confidence intervals (95% CIs) were calculated.

## RESULTS

**Greater bone-forming potency of MSCs from periosteum than from synovium.** We quantified the osteogenic potency of matched human MSC preparations from SM and periosteum. In vitro, passage 7 SM MSCs and periosteal MSCs were treated with osteogenic medium for 20 days and assessed for alkaline phosphatase activity at different time points. In both MSC populations, there was a significant increase in alkaline phosphatase activity, which peaked on day 8 and then returned to almost basal levels by day 20 (Figure 1A). A first important source of variability that we identified was the tissue of origin of MSCs. Indeed, at all time

points except days 0 and 20, periosteal MSCs displayed significantly higher levels of alkaline phosphatase activity than did SM MSCs (Figure 1A). By day 20, calcium deposits were significantly higher in periosteal MSCs than in SM MSCs (Figure 1B). Under similar conditions, human dermal fibroblasts failed to undergo osteogenesis (data not shown). These data indicate greater osteogenic potential of periosteal MSCs than SM MSCs in vitro.

To investigate whether the difference in osteogenic potential was dependent on in vitro conditions, we examined the capacity of SM MSCs and periosteal MSCs to form bone in vivo. We used an established assay consisting of seeding cells onto osteoinductive Collagraft scaffolds (composed of hydroxyapatite, tricalcium phosphate, and type I collagen, routinely used in orthopedic clinical practice) and implanting the constructs under the skin of immunodeficient nude mice (4,20). The seeding efficiency of SM MSCs and periosteal MSCs into Collagraft scaffolds was comparable (~40–70%), with no correlation between MSC seeding efficiency and bone formation in vivo. Histologically, no bone was evident at 4 weeks. At 8 weeks, areas of woven bone were observed after H&E staining of both SM MSC–seeded (Figures 1C and D) and periosteal MSC–seeded scaffolds (Figures 1E and F).

In contrast, no bone was retrieved from empty scaffolds or scaffolds seeded with expanded human dermal fibroblasts (data not shown), indicating that human MSCs are necessary for bone formation in vivo under these conditions. In situ hybridization for human Alu genomic repeats demonstrated that human nuclei were present within bone areas in both SM MSC and periosteal MSC constructs (Figure 1G).

To confirm differentiation of human MSCs into an osteoblast phenotype at the molecular level, we monitored the expression of human osteocalcin (OC) by quantitative real-time RT-PCR using human-specific primers. The levels of human OC messenger RNA (mRNA), normalized to human $\beta$-actin, were significantly higher in the periosteal MSC constructs at both 4 and 8 weeks (Figure 1H), indicating that periosteal MSCs had greater osteogenic potential in vivo than did SM MSCs.

To quantify bone formation, we measured the bone area in serial sections of MSC constructs by histomorphometry, following H&E staining. At 8 weeks, the percent area occupied by bone was significantly higher in periosteal MSC constructs than in SM MSC constructs (Figure 1I). The levels of OC mRNA detected with human-specific primers were significantly higher in periosteal MSC than in SM MSC implants (Figure 1H) and correlated significantly with the percent bone area (gradient 121.4 [95% CI 112, 131]; $R^2$ = 0.997, $P$ = 0.000) (Figure 1J).

A second source of variability within each tissue was related to the individual donor. The coefficients of variation of OC expression levels and percent bone area in vivo were 55% and 90% for SM MSCs and 36% and 41% for periosteal MSCs, respectively. This interindividual variability was not due to unreliable measurements, since within each sample, the values of OC expression and percent bone area, obtained using 2 independent systems, displayed a high degree of correlation (Figure 1J).

Calcium deposition (normalized to protein content) after 20 days of osteogenic treatment in vitro correlated significantly with both percent bone area (gradient 0.015 [95% CI 0.01, 0.02]; $R^2$ = 0.941, $P$ = 0.0000) (Figure 1K) and expression levels of human OC (normalized to human $\beta$-actin; gradient 0.0001 [95% CI 0.0001, 0.0002]; $R^2$ = 0.944, $P$ = 0.001) (Figure 1L) at 8 weeks in vivo. This indicates that, under our experimental conditions and at the specified time points, calcium deposition (normalized to protein content) in the in vitro osteogenesis assay was sufficient to measure osteogenic outcome quantitatively.

**No significant differences in growth potential and cell phenotype between synovial and periosteal MSCs.** Growth potential and cell phenotype could account for the differential bone-forming capacities of MSC populations (23). During culture expansion, the growth curves of SM MSCs and periosteal MSCs from the 4 donors tested overlapped and remained linear over at least 30 population doublings (Figure 2A). As expected, and consistent with the findings of our previous studies (4,5), there was a progressive age-associated decline in the growth rate of MSCs, which was comparable for both SM MSCs and periosteal MSCs (Figures 2B and C). We then determined semiquantitatively the length of the telomeres of SM MSCs and periosteal MSCs at passage 7, when the osteogenesis assays were carried out. Despite undetectable telomerase activity (4,5), the telomeres of the human MSC populations tested were long, comparable with those of an immortalized cell line, irrespective of donor age, and with no significant difference between the 2 tissue sources (Figure 2D). The mean ± SD telomere length was 11.50 ± 0.53 for SM MSCs and 11.45 ± 0.47 for periosteal MSCs ($P$ = 0.86).

Next, we compared the phenotype of the expanded human MSCs using fluorescence-activated cell

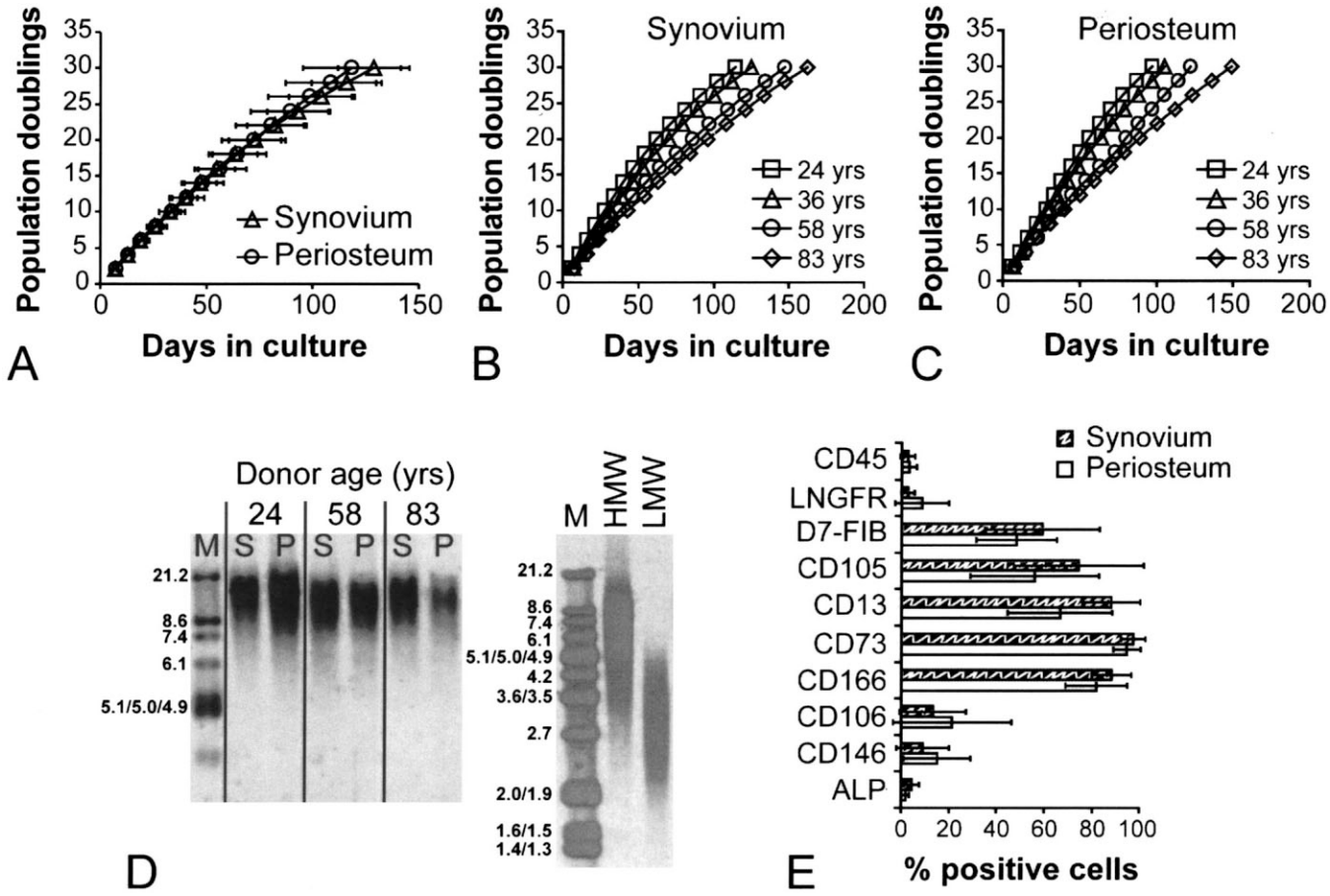


**Figure 2.** Growth potential and phenotype of SM MSCs and periosteal MSCs. **A,** Kinetics of growth of MSCs from 4 donors. The kinetics of growth were analyzed starting with the first passage. The growth curves overlapped and remained linear up to 30 population doublings, with no significant difference between SM MSCs and periosteal MSCs. **B** and **C,** Age-associated decline in the growth rates of SM MSCs (**B**) and periosteal MSCs (**C**). **D,** Southern blot analysis of telomeres. Expanded MSCs from 3 donors of different ages were analyzed by Southern blot analysis to determine the length of their telomeres. Regardless of donor age, the telomere lengths were comparable, with no significant difference between SM MSCs (S) and periosteal MSCs (P). The U937 cell line was used as a positive control (high molecular weight [HMW]; mean telomere length 10.2 kb), and HL-60 cells were used as a negative control (low molecular weight [LMW]; mean telomere length 3.9 kb). M = molecular weight marker. **E,** Surface marker phenotype of human MSCs following culture expansion. Values are the mean ± SD of 4 donors. Both SM MSCs and periosteal MSCs displayed high self-renewal capacity and a conventional MSC phenotype, and there was no significant difference between the 2 tissue sources. LNGFR = low-affinity nerve growth factor receptor (see Figure 1 for other definitions).

sorting. Both synovial and periosteal cell populations displayed the conventional MSC phenotype (3,24,25), with no significant difference in the expression levels of the cell surface markers tested (Figure 2E). Histograms are shown in Supplementary Figure 1, available on the *Arthritis & Rheumatism* Web site at http://www.mrw.interscience.wiley.com/suppmat/0004-3591/suppmat/. As expected, CD45, a marker of hematopoietic lineage cells, was not detected in any of the MSC samples tested. Expression of CD73, CD166, CD105, CD13, and D7-FIB was detected uniformly in all MSC samples. CD146 and CD106 displayed variable expression between donors, with no correlation with donor age. LNGFR was undetectable in expanded MSCs (Figure 2E), consistent with findings reported for MSCs from human bone marrow (24). To exclude osteoblast contamination or early osteogenic commitment of MSC populations, we analyzed the cell surface expression levels of the osteoblast lineage marker alkaline phosphatase (26,27). Both synovial and periosteal MSCs were negative for alkaline phosphatase (Figure 2E), consistent with the notion that they were undifferentiated MSCs with no detectable commitment to the osteogenic lineage.

**Osteogenic potency in single-cell–derived clonal populations.** MSC populations were expanded as polyclonal cultures. Thus, the different osteogenic capacities

of SM MSCs and periosteal MSCs could either result from variability in cell subset compositions of these possibly mixed cell populations or be inherent to the single MSC. To address this, we compared the osteogenic potency of single-cell–derived clonal populations obtained by limiting dilution from both synovium and periosteum. Of a total of 91 clones analyzed, 31 stopped growing prior to 10 population doublings. The remaining 60 clones displayed heterogeneous proliferation potential in vitro (Figure 3A).

To eliminate the bias of different growth rates and to compare like with like, we selected 8 clones (4 SM and 4 periosteal clones; 1 clone per tissue per donor) that displayed similar and efficient growth curves (Figure 3B) and similar telomere lengths (Figure 3C). Mean ± SD telomere length was 7.08 ± 0.63 for synovial clones and 7.53 ± 0.18 for periosteal clones ($P = 0.23$). As assessed by flow cytometry, expanded clonal populations displayed the conventional MSC phenotype (representative histograms are shown in Supplementary Figure 2, available on the *Arthritis & Rheumatism* Web site at http://www.mrw.interscience.wiley.com/suppmat/0004-3591/suppmat/). All selected clones were multipotent, capable of chondrogenic, osteogenic, and adipogenic differentiation in vitro (data not shown). After 22 population doublings, and while still in the linear phase of their growth curves, the clonal cell populations were assessed quantitatively for their capacity to undergo osteogenesis in vitro. Periosteal clones displayed a significantly greater osteogenic potential than did SM clones, as determined by alkaline phosphatase activity (Figure 3D) and calcium deposition (Figure 3E), indicating that the superior osteogenic potency of periosteal MSCs is intrinsic to the single multipotent MSC.

To investigate the molecular basis of this differential osteogenic potency and to identify potential predictors of osteogenic outcome, we examined the expression levels of osteoblast lineage genes in both SM MSC and periosteal MSC clonal populations prior to osteogenic treatment. The expression levels of type I collagen, osteoprotegerin (OPG), osteonectin, and osteopontin, normalized to GAPDH, were significantly higher in the periosteal clones than in the synovial clones, whereas there was no significant difference in the expression levels of runt-related transcription factor 2, osterix, alkaline phosphatase, bone sialoprotein, or OC (Figure 3F). The basal expression levels of osteoblast lineage genes in clonal MSCs were log scales lower than in periosteal MSCs after full osteogenic differentiation in the Collagraft scaffold in vivo (Figure 3F), indicating that prior to osteogenic treatment, neither synovial nor

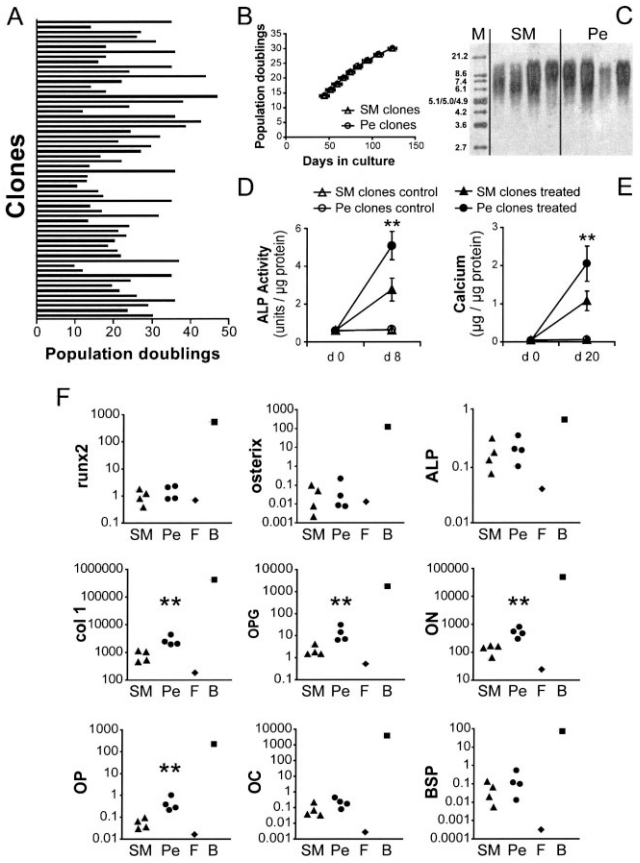


**Figure 3.** Comparison of SM MSCs and periosteal MSCs at the single-cell level. **A,** Proliferation potential of synovial and periosteal clones. Sixty clones were analyzed for their cumulative production of cells. A marked variation in proliferative capacity between individual clones is evident. **B,** Kinetics of growth of 8 selected single-cell–derived clonal MSCs from synovium and periosteum (1 clone per tissue type per donor). The growth curves were linear and overlapped. **C,** Southern blot analysis showing telomere lengths of the 4 selected SM clones and 4 selected periosteal clones. M = molecular weight marker. **D,** ALP activity on days 0 and 8 of treatment with osteogenic medium in vitro. Values are the mean ± SD of the 4 selected SM clones and 4 selected periosteal clones. ** = $P < 0.01$ versus SM MSCs. **E,** Calcium deposition on days 0 and 20. Values are the mean ± SD of the 4 selected SM clones and 4 selected periosteal clones. Periosteal clones displayed significantly greater osteogenic potential than did synovial clones. ** = $P < 0.01$ versus SM MSCs. **F,** Quantification of the results of real-time quantitative reverse transcriptase–polymerase chain reaction for osteoblast lineage genes normalized to human GAPDH in the selected culture-expanded synovial and periosteal single-cell–derived clonal populations, prior to osteogenic treatment. Data are expressed on a logarithmic scale. ** = $P < 0.01$ versus SM MSCs. RUNX-2 = runt-related transcription factor 2; F = human dermal fibroblasts (negative control); B = human periosteal MSC–Collagraft construct containing bone tissue (8 weeks in vivo), used as a reference for expression levels of osteoblast markers; col1 = type I collagen; OPG = osteoprotegerin; ON = osteonectin; OP = osteopontin; OC = osteocalcin; BSP = bone sialoprotein (see Figure 1 for other definitions).

periosteal clonal MSCs displayed an osteoblast phenotype.

**A biomarker-based mathematical model to predict MSC osteogenic potency.** Capitalizing on these results, we endeavored to identify predictors of osteogenic potency of MSCs that would be independent of the tissue source and of the donor. To this end, we evaluated the correlations between the basal gene expression levels in the 8 selected (4 synovial and 4 periosteal) clonal MSCs prior to osteogenic treatment and the values of calcium deposition at 20 days of osteogenic treatment in vitro (Table 2). In a multiple linear regression model ($R^2$ = 98%; adjusted 98%) of the individual markers studied, type I collagen proved to be the most important predictor, followed by OPG. Although the bivariate correlation between calcium and OPG was moderate ($R^2$ = 0.36), a curve fitting exercise indicated a strong quadratic trend ($R^2$ = 0.91), thus confirming OPG as a valid predictor. Calcium increased on average by 0.43 (95% CI 0.3, 0.53; $P$ = 0.000) for each unit increase in type I collagen and by 0.012 (95% CI 0.001, 0.02; $P$ = 0.04) for each unit increase in OPG. The derived model was as follows:

$$\text{Calcium/proteins} = 0.70 + 0.43 \times (\text{type I collagen/GAPDH}) + 0.012 \times (\text{OPG/GAPDH})$$

There was no interaction with the type of clonal MSC population, indicating that this model can predict osteogenic outcome regardless of the tissue of origin of MSCs.

The model showed excellent agreement with the actual calcium scale (Figure 4A). The Bland and Altman plot (Figure 4B) proved that the bias was independent of the level of calcium assessed (the ICC was 98%). The estimate of the average discrepancy in relation to the actual calcium scale was 0.01, with an SD of 0.09, yielding 95% limits of agreement of −0.07 (95% CI −0.08, −0.06) to 0.09 (95% CI 0.08, 0.10).

**Table 2.** Correlation of gene expression levels with calcium deposition*

| Gene | R | *P* |
|---|---|---|
| Runx2 | 0.108 | 0.400 |
| Osterix | 0.164 | 0.349 |
| ALP | 0.463 | 0.124 |
| Type I collagen | 0.973 | 0.000 |
| OPG | 0.598 | 0.059 |
| Osteonectin | 0.904 | 0.001 |
| Osteopontin | 0.322 | 0.218 |
| Osteocalcin | 0.923 | 0.001 |
| BSP | 0.338 | 0.206 |

* Basal expression levels of osteoblast lineage genes in clonal mesenchymal stem cells prior to osteogenic treatment, and levels of calcium deposition (normalized to protein content) at 20 days of osteogenic treatment in vitro were measured, and correlations determined. See Table 1 for definitions.

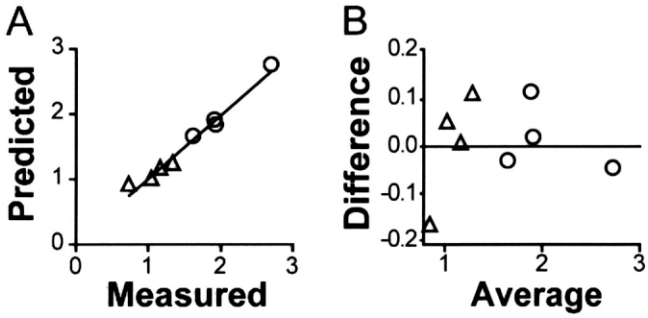


**Figure 4.** Analysis of the mathematical model predicting osteogenic outcome. **A,** Plot of calcium predicted with the model versus calcium measured, and line of equality. **B,** Bland and Altman plot of the difference (measured minus predicted; bias) versus the average (measured and predicted). Triangles represent SM MSCs, and circles represent periosteal MSCs. See Figure 1 for definitions.

## DISCUSSION

Several studies have demonstrated the therapeutic utility of MSCs in humans (6–8,28–31). However, donor-related variability and inconsistency of MSC preparations limit standardization and impede comparisons of clinical study outcomes. In this proof-of-concept study, we proposed a strategy for tackling this problem. We developed a simple mathematical model based on the expression of only 2 biomarkers, type I collagen and OPG, which predicts the osteogenic potency of adult human MSC preparations from synovium and periosteum, independently of donor-related variables and tissue source.

The mathematical model was obtained using single-cell–derived clonal populations. As with clonal populations, periosteal polyclonal MSCs displayed a significantly greater osteogenic potency than did synovial polyclonal MSCs. However, within each tissue source of MSCs, there was no statistically significant difference in the osteogenic outcome between polyclonal and clonal cell populations. In spite of this, when we applied the mathematical model to polyclonal synovial or periosteal MSC populations, it yielded an ICC of 25%, thus showing low predictive power. In addition, it was not possible to generate by regression analysis any model predictive of the osteogenic outcome of polyclonal cell populations, at least with the molecular markers tested. A possible explanation is that in poly-

clonal mixed cell populations, noncompetent, nonclonogenic cells would influence the overall gene expression prior to osteogenic treatment, but are subsequently lost during selective osteogenic conditions. In support of this hypothesis, in the osteogenic cultures a large proportion of cells underwent apoptosis within the first few days of treatment, resulting in the selection of a subpopulation that underwent osteogenesis (data not shown).

As reported with single-cell–derived colonies of bone marrow–derived stromal cells (32–34), synovial and periosteal clonal populations became heterogeneous during culture expansion, as determined by flow cytometry for the cell surface markers tested (Supplementary Figure 2). Nonetheless, the growth curves and the osteogenic outcomes of individual clonal populations were distinct, and it was possible to predict their osteogenic potential using molecular markers. The phenotypic heterogeneity within each clonal population may be due to the different functional status of the individual cells of the single-cell progeny (e.g., different phases of the cell cycle, symmetric or asymmetric cell division, or different stages of differentiation). However, in spite of the phenotypic heterogeneity during culture expansion, clones would maintain distinct, possibly inherent biologic features. The coexistence, in different proportions, of clones with diverse osteogenic potential within the same polyclonal population would result in a variability too complex to be predicted by our marker analysis.

We are aware that the use of clonal populations in the clinic would be impractical and costly, and therefore, we do not advocate the use of our model for quality control of MSC populations for clinical use with the current technologies. However, our biomarker-based model represents a biologic platform upon which to devise strategies for the prospective purification of MSC subpopulations with predictable and consistent bone-forming potency independently of the donor and tissue source. Such purification, which could be either from fresh synovial/periosteal tissue digests or from expanded polyclonal cell populations, would not only increase the consistency of MSC preparations for clinical use, but also facilitate the estimation of their potency by using biomarkers, thus allowing standardization of therapeutic protocols using MSCs.

Periosteal MSCs formed more bone in vivo than did SM MSCs, as determined by histomorphometry. The bone tissue retrieved appeared to be largely of human origin. Although we do not exclude contribution of the mouse host to bone formation in vivo, the difference in bone amount is unlikely to be solely due to periosteal MSCs having a greater capacity for recruiting mouse host osteoprogenitor cells, since the levels of OC mRNA detected with human-specific primers were significantly higher in periosteal MSC implants than in SM MSC implants and correlated significantly with the percent bone area. Notably, no bone was retrieved from empty scaffolds or scaffolds seeded with expanded human dermal fibroblasts, indicating that human MSCs are necessary for bone formation in vivo under these experimental conditions.

The development of a biomarker-based model that predicts the bone-forming potency of human MSC preparations is of considerable clinical relevance. It may facilitate the selection of individuals that qualify for an MSC-based bone repair approach. It may also help identify the best source and preparation protocol of human MSCs or adjust the dose in bone-forming MSC units from patient to patient. It remains to be investigated whether the same formula can be applied to MSC preparations from other tissue sources, such as bone marrow, or to any other stem cell preparations, whether embryonic, fetal, or adult. We predict that, in addition to the properties intrinsic to the cell preparation, other factors such as inflammation, biomechanics, and patient comorbidity will influence orthotopic bone formation and clinical outcome. Preclinical studies and clinical trials of bone repair using MSC-based protocols will thus be necessary for prospective validation of our potency assays and related model.

The generation of consistent MSC-based therapeutic protocols is a prerequisite for translating these technologies into routine clinical application. There is evidence that MSCs from mismatched donors could be poorly immunogenic in recipients in some in vivo systems (35,36). Also, the induction of tolerance to allogeneic stem cells is a field of intense investigation (37). Once the immunologic barriers are overcome, potency assays and related quality control measures will provide a solid basis for establishing batches of certified stem cell products with specific clinical indications for allogeneic transplantation. This approach will increase consistency and decrease costs of MSC therapies, thus accelerating translation to routine clinical use.

## ACKNOWLEDGMENT

We thank the staff of the mortuary at the University Hospitals, Katholieke Universiteit Leuven.

## AUTHOR CONTRIBUTIONS

Dr. De Bari had full access to all of the data in the study and takes responsibility for the integrity of the data and the accuracy of the data analysis.

**Study design.** De Bari, Dell'Accio, Fisk, Luyten, Pitzalis.
**Acquisition of data.** De Bari, Dell'Accio, Karystinou, Guillot, Jones, McGonagle, Khan, Archer.
**Analysis and interpretation of data.** De Bari, Dell'Accio, Guillot, Fisk, Jones, Khan, Archer, Mitsiadis, Donaldson.
**Manuscript preparation.** De Bari, Dell'Accio, Guillot, Fisk, Jones, McGonagle, Khan, Mitsiadis, Donaldson, Luyten, Pitzalis.
**Statistical analysis.** De Bari, Dell'Accio, Jones, Khan, Donaldson.

## REFERENCES


1. Rosenzweig A. Cardiac cell therapy—mixed results from mixed cells. N Engl J Med 2006;355:1274–7.
2. Prockop DJ. Marrow stromal cells as stem cells for nonhematopoietic tissues. Science 1997;276:71–4.
3. Pittenger MF, Mackay AM, Beck SC, Jaiswal RK, Douglas R, Mosca JD, et al. Multilineage potential of adult human mesenchymal stem cells. Science 1999;284:143–7.
4. De Bari C, Dell'Accio F, Vanlauwe J, Eyckmans J, Khan IM, Archer CW, et al. Mesenchymal multipotency of adult human periosteal cells demonstrated by single-cell lineage analysis. Arthritis Rheum 2006;54:1209–21.
5. De Bari C, Dell'Accio F, Tylzanowski P, Luyten FP. Multipotent mesenchymal stem cells from adult human synovial membrane. Arthritis Rheum 2001;44:1928–42.
6. Quarto R, Mastrogiacomo M, Cancedda R, Kutepov SM, Mukhachev V, Lavroukov A, et al. Repair of large bone defects with the use of autologous bone marrow stromal cells. N Engl J Med 2001;344:385–6.
7. Vacanti CA, Bonassar LJ, Vacanti MP, Shufflebarger J. Replacement of an avulsed phalanx with tissue-engineered bone. N Engl J Med 2001;344:1511–4.
8. Warnke PH, Springer IN, Wiltfang J, Acil Y, Eufinger H, Wehmoller M, et al. Growth and transplantation of a custom vascularised bone graft in a man. Lancet 2004;364:766–70.
9. Wang T, Dang G, Guo Z, Yang M. Evaluation of autologous bone marrow mesenchymal stem cell-calcium phosphate ceramic composite for lumbar fusion in rhesus monkey interbody fusion model. Tissue Eng 2005;11:1159–67.
10. Phinney DG, Kopen G, Righter W, Webster S, Tremain N, Prockop DJ. Donor variation in the growth properties and osteogenic potential of human marrow stromal cells. J Cell Biochem 1999;75:424–36.
11. Kuznetsov SA, Mankani MH, Gronthos S, Satomura K, Bianco P, Robey PG. Circulating skeletal stem cells. J Cell Biol 2001;153:1133–40.
12. Batouli S, Miura M, Brahim J, Tsutsui TW, Fisher LW, Gronthos S, et al. Comparison of stem-cell-mediated osteogenesis and dentinogenesis. J Dent Res 2003;82:976–81.
13. Hui JH, Li L, Teo YH, Ouyang HW, Lee EH. Comparative study of the ability of mesenchymal stem cells derived from bone marrow, periosteum, and adipose tissue in treatment of partial growth arrest in rabbit. Tissue Eng 2005;11:904–12.
14. Matsubara T, Suardita K, Ishii M, Sugiyama M, Igarashi A, Oda R, et al. Alveolar bone marrow as a cell source for regenerative medicine: differences between alveolar and iliac bone marrow stromal cells. J Bone Miner Res 2005;20:399–409.
15. Sakaguchi Y, Sekiya I, Yagishita K, Muneta T. Comparison of human stem cells derived from various mesenchymal tissues: superiority of synovium as a cell source. Arthritis Rheum 2005;52:2521–9.
16. De Bari C, Pitzalis C, Dell'Accio F. Reparative medicine: from tissue engineering to joint surface regeneration. Regen Med 2006;1:59–69.
17. Luyten FP, Dell'Accio F, De Bari C. Skeletal tissue engineering: opportunities and challenges. Best Pract Res Clin Rheumatol 2001;15:759–69.
18. Harley CB, Futcher AB, Greider CW. Telomeres shorten during ageing of human fibroblasts. Nature 1990;345:458–60.
19. Dell'Accio F, De Bari C, Luyten FP. Molecular markers predictive of the capacity of expanded human articular chondrocytes to form stable cartilage in vivo. Arthritis Rheum 2001;44:1608–19.
20. Dell'Accio F, De Bari C, Luyten FP. Microenvironment and phenotypic stability specify tissue formation by human articular cartilage-derived cells in vivo. Exp Cell Res 2003;287:16–27.
21. De Bari C, Dell'Accio F, Luyten FP. Failure of in vitro–differentiated mesenchymal stem cells from the synovial membrane to form ectopic stable cartilage in vivo. Arthritis Rheum 2004;50:142–50.
22. De Bari C, Dell'Accio F, Vandenabeele F, Vermeesch JR, Raymackers JM, Luyten FP. Skeletal muscle repair by adult human mesenchymal stem cells from synovial membrane. J Cell Biol 2003;160:909–18.
23. Muraglia A, Cancedda R, Quarto R. Clonal mesenchymal progenitors from human bone marrow differentiate in vitro according to a hierarchical model. J Cell Sci 2000;113(Pt 7):1161–6.
24. Jones EA, Kinsey SE, English A, Jones RA, Straszynski L, Meredith DM, et al. Isolation and characterization of bone marrow multipotential mesenchymal progenitor cells. Arthritis Rheum 2002;46:3349–60.
25. Jones EA, English A, Henshaw K, Kinsey SE, Markham AF, Emery P, et al. Enumeration and phenotypic characterization of synovial fluid multipotential mesenchymal progenitor cells in inflammatory and degenerative arthritis. Arthritis Rheum 2004;50:817–27.
26. Gronthos S, Zannettino AC, Graves SE, Ohta S, Hay SJ, Simmons PJ. Differential cell surface expression of the STRO-1 and alkaline phosphatase antigens on discrete developmental stages in primary cultures of human bone cells. J Bone Miner Res 1999;14:47–56.
27. Stewart K, Walsh S, Screen J, Jefferiss CM, Chainey J, Jordan GR, et al. Further characterization of cells expressing STRO-1 in cultures of adult human bone marrow stromal cells. J Bone Miner Res 1999;14:1345–56.
28. Wakitani S, Mitsuoka T, Nakamura N, Toritsuka Y, Nakamura Y, Horibe S. Autologous bone marrow stromal cell transplantation for repair of full-thickness articular cartilage defects in human patellae: two case reports. Cell Transplant 2004;13:595–600.
29. Wakitani S, Imoto K, Yamamoto T, Saito M, Murata N, Yoneda M. Human autologous culture expanded bone marrow mesenchymal cell transplantation for repair of cartilage defects in osteoarthritic knees. Osteoarthritis Cartilage 2002;10:199–206.
30. Horwitz EM, Gordon PL, Koo WK, Marx JC, Neel MD, McNall RY, et al. Isolated allogeneic bone marrow-derived mesenchymal cells engraft and stimulate growth in children with osteogenesis imperfecta: implications for cell therapy of bone. Proc Natl Acad Sci U S A 2002;99:8932–7.
31. Horwitz EM, Prockop DJ, Fitzpatrick LA, Koo WW, Gordon PL, Neel M, et al. Transplantability and therapeutic effects of bone marrow-derived mesenchymal cells in children with osteogenesis imperfecta. Nat Med 1999;5:309–13.
32. Colter DC, Class R, DiGirolamo CM, Prockop DJ. Rapid expansion of recycling stem cells in cultures of plastic-adherent cells from human bone marrow. Proc Natl Acad Sci U S A 2000;97:3213–8.
33. Colter DC, Sekiya I, Prockop DJ. Identification of a subpopulation of rapidly self-renewing and multipotential adult stem cells in colonies of human marrow stromal cells. Proc Natl Acad Sci U S A 2001;98:7841–5.
34. Prockop DJ. Further proof of the plasticity of adult stem cells and their role in tissue repair. J Cell Biol 2003;160:807–9.
35. Arinzeh TL, Peter SJ, Archambault MP, van den Bos C, Gordon S, Kraus K, et al. Allogeneic mesenchymal stem cells regenerate

bone in a critical-sized canine segmental defect. J Bone Joint Surg Am 2003;85-A:1927–35.
36. Rodriguez AM, Pisani D, Dechesne CA, Turc-Carel C, Kurzenne JY, Wdziekonski B, et al. Transplantation of a multipotent cell population from human adipose tissue induces dystrophin expression in the immunocompetent mdx mouse. J Exp Med 2005;201:1397–405.
37. Fairchild PJ, Cartland S, Nolan KF, Waldmann H. Embryonic stem cells and the challenge of transplantation tolerance. Trends Immunol 2004;25:465–70.

DOI 10.1002/art.23236

*Clinical Image: Fibrodysplasia ossificans progressiva seen on three-dimensional computed tomography*

The patient, a 28-year-old woman, was admitted to our hospital with trismus, abnormal soft tissue tumors, and diffuse ankylosis of the limbs and trunk. These symptoms had progressed following 2 surgeries, 19 years and 23 years previously. Whole-body 3-dimensional computed tomography scanning revealed diffuse calcification over the soft tissue of the neck, both arms, chest wall, and left thigh. The patient was diagnosed as having fibrodysplasia ossificans progressiva, a rare inherited disease characterized by progressive soft tissue ossification occurring after minor injuries. Three-dimensional computed tomography can be a useful tool for diagnosis of this condition.

Chien-Hsueh Tung, MD
Ning-Sheng Lai, MD, PhD
*Buddhist Tzu Chi General Hospital*
*Dalin, Chia-yi, Taiwan*